Int J Adv Manuf Technol
DOI 10.1007/s00170-016-8940-6

ORIGINAL ARTICLE

Smooth particle hydrodynamics study of surface defect machining for diamond turning of silicon

Amir Mir[1] · **Xichun Luo**[1] · **Amir Siddiq**[2]

Received: 9 November 2015 / Accepted: 16 May 2016

Abstract This paper presents the feasibility study of potential application of recently developed surface defect machining (SDM) method in the fabrication of silicon and similar hard and brittle materials using smooth particle hydrodynamics (SPH) simulation approach. Simulation study of inverse parametric analysis was carried out to determine the Drucker-Prager (DP) constitutive model parameters of silicon by analysing the deformed material response behaviour using various DP model parameters. Indentation test simulations were carried out to perform inverse parametric study. SPH approach was exploited to machine silicon using conventional and surface defect machining method. To this end, we delve into opportunities of exploiting SDM through optimised machining quality, reduced machining time and lowering cost. The results of the conventional simulation were compared with the results of experimental diamond turning of silicon. In the SPH simulations, various types of surface defects were introduced on the workpiece prior to machining. Surface defects were equally distributed on the top face of the workpiece. The simulation study encompasses the investigation of chip formation, resultant machining forces, stresses and hydrostatic pressure with and without SDM. The study reveals the SDM process is an effective technique to manufacture hard and brittle materials as well as facilitate increased tool life. The study also divulges the importance of SPH evading the mesh distortion problem and offer natural chip formation during machining of hard and brittle materials.

Keywords Surface defect machining · Diamond turning · Silicon · SPH

1 Introduction

Silicon has great importance in optoelectronics, semiconductor, MEMS, space and defense industries due to its great electro-mechanical properties, great high-temperature strength and low thermal expansion properties. Silicon has been widely used as a semiconductor in computer peripherals, camera technology and in microelectronic industries. However, silicon with these enviable characteristics is correspondingly difficult to machine material and brittle fracture is an impediment to high surface quality during machining.

The materials believe to undergo brittle failure when at yield point fail to resist load prematurely without any ductile deformation. Machining brittle materials through plastic deformation was first narrated by King and Tabor [1]. During the abrasive wear of rocks, they observed plastic deformation of material along with typical brittle fracture. In plastic deformation, shear stress exceeds the critical value of material-dependent shear strength and deformation initiate due to slip in specific closed-packed crystallographic planes in specific directions.

Brittle materials such as germanium [2], silicon [3] and silicon carbide [4] have been found to deform plastically and behave like metals due to the formulation of high-pressure phase transformation (HPPT) at tool-chip interface in which they transform structurally into different phases. The brittle-ductile criterion is also highly dependent on other cutting parameters such as critical depth of cut, tool geometry and feed.

✉ Xichun Luo
Xichun.luo@strath.ac.uk

[1] Centre for Precision Manufacturing, Department of Design, Manufacture and Engineering Management, University of Strathclyde, Glasgow, UK

[2] Department of Physical Sciences, University of Aberdeen, Aberdeen, UK

Published online: 02 June 2016

Blake and Scattergood propounded the machining model of brittle materials in ductile mode based on critical chip thickness criteria [5].

Different techniques such as X-ray diffraction, optical and various others have been exploited to study the phase transformation of silicon. Silicon retains diamond cubic structure in its natural state under normal conditions with a lattice spacing of 5.430710 Å [3]. The transition of crystalline silicon transpires at ~11–12 GPa into β-sn metallic phase along with volume reduction. Above 14 Gpa, primitive hexagonal phase appears which sustains until reaching 40 GPa pressure at which it transforms into the hexagonal close-packed structure. With different loading and unloading conditions, silicon has been found to transmute into several other phases.

Ultra-precision techniques have been developed beyond lapping and polishing to fabricate soft and ductile material products with optical surface finish, e.g. using single-point diamond turning, diamond micro-milling and various others. Nevertheless, while machining hard and brittle materials such as silicon, silicon carbide, germanium etc., these techniques suffer from high tool wear and brittle fracture of workpiece material due to superfluous mechanical, chemical and thermal interaction of tool and workpiece material [6, 7]. Various seminal machining methodologies have been exploited to improve these ultra-precision techniques to achieve reduced tool wear and improved surface finish. Table 1 lists few of the developed methodologies successfully tested against some of the hard and brittle materials.

In an effort to improve the machinability of hard materials, the SDM method was recently developed and comparatively tested in hard turning of AISI 4340 steel using conventional and SDM method [21]. The hard turning trials of AISI 4340 were carried out on Mori-Seiki SL-25 Y CNC lathe using CBN tool inserts with and without surface defects. Surface defects in the form of equally spaced holes with 0.9 mm diameter and 0.1 mm depth were generated on the workpiece surface using Trumpf (CO_2) laser machine with 2.7 kW peak power. The trial results revealed the potential of SDM in achieving improved surface roughness, reduced cutting temperature and lower cutting forces and consequently reduced tool wear.

The elementary concept of SDM is to reduce the surface strength of the workpiece in the chip formation zone. This method entails the generation of surface defects offline at a depth less than the uncut chip thickness using sophisticated mechanical, thermal or any other suitable methods before the actual machining. In SDM, material removal results in weak interface layer on the top face which is of critical importance in stress degradation. Material defects lead to discontinuous and broken chips and result into reduced cutting temperature and lower tool wear [22]. The SDM method offer reduction in the shear strength reduced residual stresses and reduced temperature which motivate better surface finish and less tool wear.

The choice of selecting the surface defects generation method is based on low cost and time, damage control and its dependence on material machinability. Surface defects can be generated using laser as well as different types of patterning tools with different structures. Different structures induce different chip flow type and direction and offer varied resistance to cutting and therefore carry significant importance in the deformation mechanism. The damage can be introduced on the workpiece surface in the form of holes, multi-shaped grooves, channels and various other structures. The shape of these defects or structures may differently contribute to reduction in cutting temperature, cutting resistance and machining energy and therefore various defects should be tested for comparison.

Nevertheless, trials of these techniques to understand the machining mechanism are costly to implement due to expensive tooling, equipment and time cost. Finite element simulation provides cost effective, time efficient and detailed analysis solution to this problem. In the first part of this paper, SPH approach is discussed. In the second part, inverse parametric analyses were performed to determine the DP parameters of silicon. In the next section, SPH simulation model was developed for silicon subjected to diamond turning. The SPH

Table 1 Selected methodologies to improve machining mechanism and tool wear

Conventional machining	Improved technique	Methodology	Workpiece material /tool material
Diamond turning	Swivel machining	Tool rotation	SiC/diamond [8]
Diamond turning	Surface modification	Amorphous structure on surface	SiC/diamond [9]
Micro-milling	Micro-milling tool development	Structures on cutting edges	Ceramics/diamond [10]
Turning, milling, drilling, grinding	Cryogenic machining	Liquid nitrogen [11], liquid CO_2 [12]	Titanium, tantalum/CBN, PCBN, hardened steel/CBN [13]
Turning, drilling, grinding	Vibration-assisted machining	Hydraulic vibrator, piezo and magneto actuator, 1-D and 2-D VAM [14]	Mild steel/carbide [15], hardened steel/diamond [16]
Turning, milling, drilling	Laser-assisted machining	CO_2laser, Nd/YAG [17]	Tool steel/CBN [18], titanium [19], silicon/diamond [20] SiC/diamond

model was then validated with experimental work. Further SPH simulations were carried out with conventional and SDM method to demonstrate the effectiveness of SDM approach. The results of SDM simulations were compared with conventional simulation model and experimental diamond turning of silicon.

2 SPH-based simulation of silicon

Silicon offers spatially different mechanical properties under varying loading and temperature conditions. Typically, machining occurs with strain rates of 10^3 to 10^6 s^{-1}, results in extreme deformation [23].

Finite element analysis of metal cutting using Lagrangian [24, 25], Eulerian and Arbitrary Lagrangian-Eulerian [26] approaches have been extensively exploited. However, machining of hard materials using positive and particularly negative rake angle tools is still a challenge due to high mesh distortion. Figure 1 illustrates the mesh distortion issue in machining hard materials. Lagrangian method evolved to meshless particle methods providing a solution to mesh distortion in large deformation processes. Particle methods offer connectivity-free nodes that eliminate the problem of mesh distortion due to connectivity restrictions in mesh-based methods during large deformation. The main particles methods exploited for machining simulations include Element-Free Galerkin Method (EFGM), Finite Pointset Method (FPM) and SPH method. Although these particle methods serve many common features, their approximation criteria are different. Although EFG offers solution accuracy to both explicit and implicit problems surpassing to SPH which is more efficient in explicit applications, the method is slower than SPH [27]. FPM method mainly employed for glass forming simulations and later adopted for cutting simulations [28]. Considering an efficient approach in terms of accuracy and computational cost for cutting process, SPH employed in this paper to simulate the diamond turning process of silicon.

2.1 Smooth particle hydrodynamics

SPH approach was first developed by Gingold and Monaghan in 1977 [29] for astrophysics applications. SPH uses kernel approximation to approximate field variables and properties in the domain (Fig. 2).

SPH approximate field variables at any particle by classical summation of smoothing function values of neighbouring particles within a sphere of influence. The length that defines the sphere of influence is based on smoothing length, and it is the maximum distance to which the interaction can occur.

$$f(x) \cong \sum_j^n \frac{(m_b)}{\rho_b} f_b W(|X - X_b|, h) \quad (1)$$

Where $f(x)$ is a scalar function and subscript b represents the neighbouring particle of the particle a for which field variables need to be approximated. W is smoothing Kernel function with radius h, called smoothing length. m_b and ρ_b are mass and densities of particle b. X_b is the location of particle b with its value f_b. In the SPH method, all particles have physical degree of freedom and each particle movement is influenced by its neighbouring particles located within the sphere of influence of radius r which is two times the smoothing length, 2 h. The particles beyond the area of influence do not contribute to the intrinsic property of cohesion on the particle of interest. In SPH formulation, particles interact with each other based on defined constitutive equations. SPH has also successfully been exploited in metal forming [30], metal cutting, indentation [31], fracture mechanics [32], geomechanics [33] and structural mechanics [34] studies.

In comparison with FEM, SPH approach was found less efficient in studying processes with tensile instability [35] or small deformation processes. Nevertheless, it has been found more effective to study large deformation processes than Lagrangian mesh-based approach. SPH approach has also been found to perform in an analogous manner to FEM following sensitivity analysis of particle resolution, mass-scaling and better than FEM in interface friction criteria [36]. In metal cutting processes, SPH method has been used to study chip

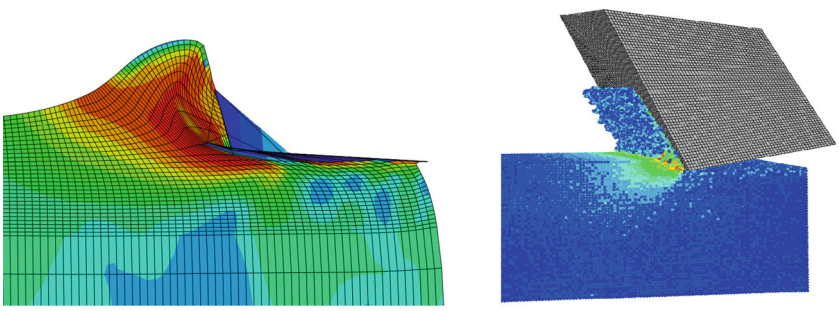

Fig. 1 Chip formation comparison in SPH and mesh-based approach

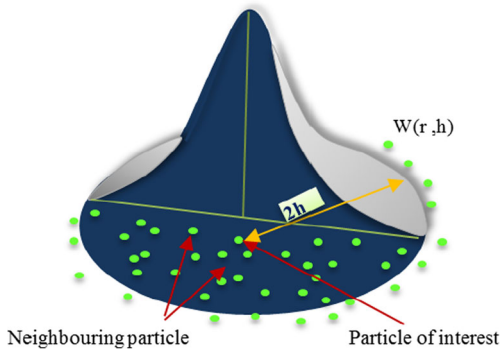

Fig. 2 SPH kernel approximation

formation of soft metals such as copper [37], aluminium [38] as well hard materials such as titanium alloys [39]. Limido et al. [40] conducted a comparative study of chip morphology of aluminium alloy and steel using 2D SPH approach, classical Lagrangian FEM and experimental approach. They found realistic chip formation and proportional cutting forces using SPH approach for both materials. Calamaz et al. [41] employed SPH approach to investigate the effect of tool wear on the variation of chip formation of titanium alloy Ti6A14V and experimentally validated the results.

Machining simulation of soft metals can be achieved using mesh-based FEM method. However, chip formation of hard materials such as silicon and silicon carbide is difficult to achieve and becomes impractical when using higher negative rake angle tools. Silicon being one of the hardest and pressure-dependent materials and due to the unavailability of high strain rate, stress-strain data have never been simulated (in the author's knowledge) for cutting process using SPH. SPH method is adopted in this paper to perform cutting simulation of silicon using appropriate pressure-dependent constitutive DP model.

2.2 Determination of Drucker-Prager parameters for SPH model

In order to study the deformation behaviour of silicon in the simulation of diamond turning, DP model was considered constitutive criteria. DP model explicates the material response behaviour of granular-like soils, rocks and other alike pressure-dependent constitutive materials. The machining response behaviour of pressure-dependent materials can be expressed in terms of strength that increases with increasing pressure. The compressive strength of silicon is higher than its tensile strength [42], which is an elementary criterion of using DP model. Under certain hydrostatic stress, the material is found to behave in ductile mode rather than brittle fracture. This behaviour clearly predicts an increase in strength of silicon under loading conditions. In order to implement DP model to simulate deformation behaviour of silicon, the compressive crushing of concrete can be replaced by the compressive plasticity of silicon and tensile dilatancy of concrete be ignored [43].

Experimental uniaxial and triaxial tests are required to obtain the constitutive parameters of materials for different versions of DP model. No experimental triaxial compression and tension data is available for silicon in the author's knowledge. In the absence of experimental data, numerical parameter optimization techniques can be used to obtain these parameters. However, the resultant parameters from optimization techniques are highly dependent on the initial assumption. In this work, an inverse parametric analysis method was adopted to determine the DP material parameters of silicon. Indentation test simulations were carried out over a range of various DP model parameters systematically chosen to acquire the required agreement between experiment and simulation results.

2.2.1 Drucker-Prager model

Since the von Mises yield criterion implies the dependence of material yielding solely on second deviatoric stress tensor J_2 and is independent of the first stress invariant I_1, the yielding sensitivity to hydrostatic stress tensor is not incorporated into pressure-sensitive materials. Drucker and Prager in 1952 [44] proposed a model to address the effect of mean (hydrostatic) stress for pressure-sensitive materials which von Mises yield criterion failed to address. The proposition acknowledged as Drucker-Prager model (also known as extended von Mises model). The Mohr-Coulomb and DP model with its yield surface are presented in Fig. 3. DP theory in principle is also a modified form of Mohr-Coulomb's theory. The DP yield criterion is expressed as:

$$f(I_1, J_2) = \alpha I_1 + \sqrt{J_2} - d = 0 \tag{2}$$

Where I_1 is the first invariant of stress tensor and J_2 is the second invariant of the deviatoric stress tensor. α is the pressure sensitivity coefficient, and d is known as the cohesion of the material. In DP model, the yield surface is the function of pressure and J_2.

The pressure-dependent linear DP yield function has also been expressed in three stress invariants [45] and inscribed as

$$f = t - p\tan\beta - c = 0 \tag{3}$$

Where p is the equivalent pressure stress and c is the material parameter known as the cohesion of the material. The term $\tan\beta$ represents the yielding sensitivity to hydrostatic pressure, and β itself is the slope of the linear yield surface

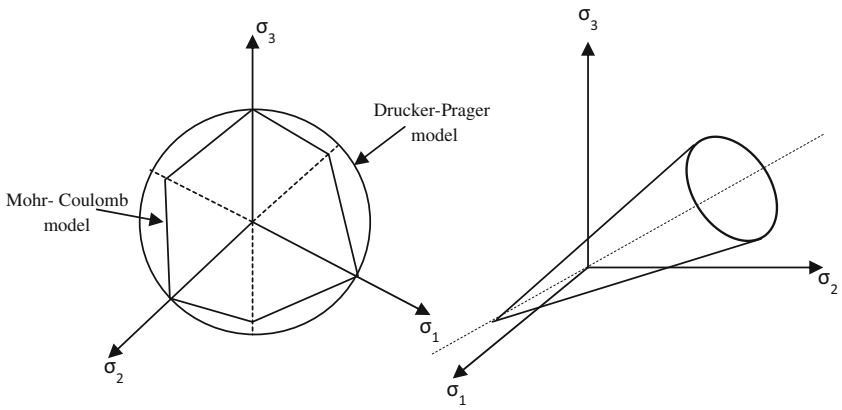

Fig. 3 Drucker-Prager model: **a** Mohr-coulomb and DP model in deviatoric plane and **b** DP yield surface

in meridional *p–t* stress plane and also known as friction angle of the material. The parameter *t is* deviatoric effective stress and expressed as

$$t = \frac{1}{2}q\left[1+\frac{1}{k}-\left(1-\frac{1}{k}\right)\left(\frac{r}{q}\right)^3\right] \tag{4}$$

and for uniaxial compression

$$C = \left(1-\frac{1}{3}\tan\beta\right)\sigma_c \tag{5}$$

Where *K* is the ratio of yield stress in the triaxial tension to triaxial compression, *q* is von Mises equivalent stress and *r is* the third invariant of deviatoric stress.

The evolution of equivalent plastic strain can be expounded using flow rule during deformation and provides the plastic strain relevance to stress components. Flow rule is stated in terms of plastic strain rate in the form of the following equation

$$d\varepsilon_{ij}^{p} = d\lambda\frac{\partial f}{\partial \sigma_{ij}} \tag{6}$$

In Abaqus, the flow potential is written in the form as

$$g = t - p\tan\psi \tag{7}$$

Where *g* is the flow potential and Ψ is dilation angle in the *p–t* plane.

2.2.2 Inverse analysis to find DP parameters

It is observed numerically that plastic zone of the pressure-sensitive material is more expanded in width and depth than that of pressure-insensitive materials [46]. High compressive strength and high stiffness of silicon make it hard to explicate its behaviour under indentation. Phase transformation of silicon from diamond cubic to *β–s* as well as in other forms is generally accompanied by micro-cracking.

Scratch tests [47], as well as various indentation tests with different types of indenters including Berkovich [48] and spherical [49], have been conducted to determine the phase transformation of silicon under different loading and unloading conditions. The elastic-plastic indentation is regarded as a complex process due to the involvement of nonlinear constitutive equations and various other variables. Indentation load and unloading rate define the formation of final phases of silicon in indentation test. DP parameters were optimised to match the load-displacement curve of finite element simulation with the experimental results [50].

In DP model, yielding depends on hydrostatic pressure and increasing confining pressure cause increase in material strength. In the experimental indentation tests [50], a sphero-conical diamond indenter with 90° included angle and tip radius of 13.5 μm was used to perform indentation on silicon sample. In order to avoid size effect [51], the

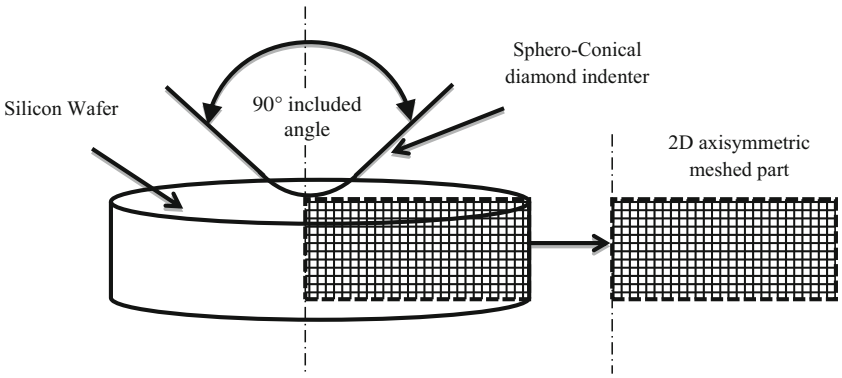

Fig. 4 Schematic of 2D axisymmetric indentation model

Table 2 Systematic selection of Drucker-Prager properties

Simulation	DP property	Friction angle β	Flow stress ratio K	dilation angle Ψ
1	Property 1	20	0.82	−10
2	Property 2	20	0.82	−18
3	Property 3	20	0.82	−4
4	Property 4	20	0.82	−14
5	Property 5	14	0.82	−10
6	Property 6	12	0.82	−10
7	Property 7	12	0.98	−10
8	Property 8	20	0.82	10
9	Property 9	24	0.82	−16
10	Property 10	26	0.82	−20
11	Property 11	28	0.82	−20

diamond indenter radius, silicon wafer thickness, indentation depth, loading and unloading conditions were kept identical to the experimental conditions. In experimental work, Si wafer with (111) crystal orientation was subjected to indentation with the conical-spherical indenter. In the simulation study, both the diamond indenter and silicon specimen were modelled axisymmetric to circumvent the computational cost. The indented silicon was modelled as a 2D axisymmetric deformable part using four-node axisymmetric element CAX4R. Figure 4 shows the schematic of the 2D axisymmetric indentation test.

A smooth refined mesh is selected at and near the contact area of the specimen to avoid any discrepancy in the computation. In order to reduce unnecessary computational time due to excessive mesh density while maintaining good simulation accuracy, a convergence test study was conducted. The von Mises stresses were used as an indicator to obtain satisfactory mesh refinement in the convergence test. The total number of elements recorded for silicon was 20,416. The material properties with an elastic modulus of 155 GPa and Poison's ratio of 0.2 were used based on experimentally measured values. The diamond indenter was modelled as rigid part with 13.5 μm edge radius and 90° included angle similar to the one used in the experimental indentation. The silicon workpiece is indented at a depth of 1100 nm to obtain and compare reaction forces with experimental results. Penalty

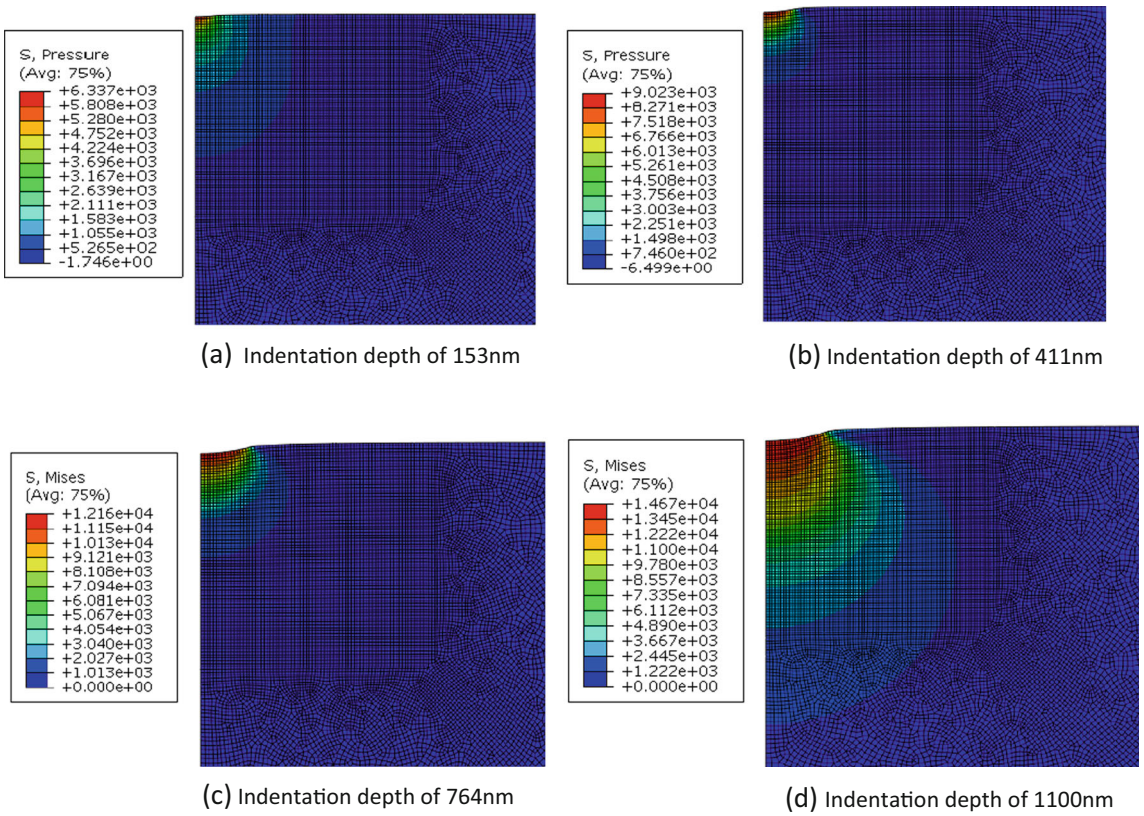

Fig. 5 Hydrostatic pressure at different indentation depths

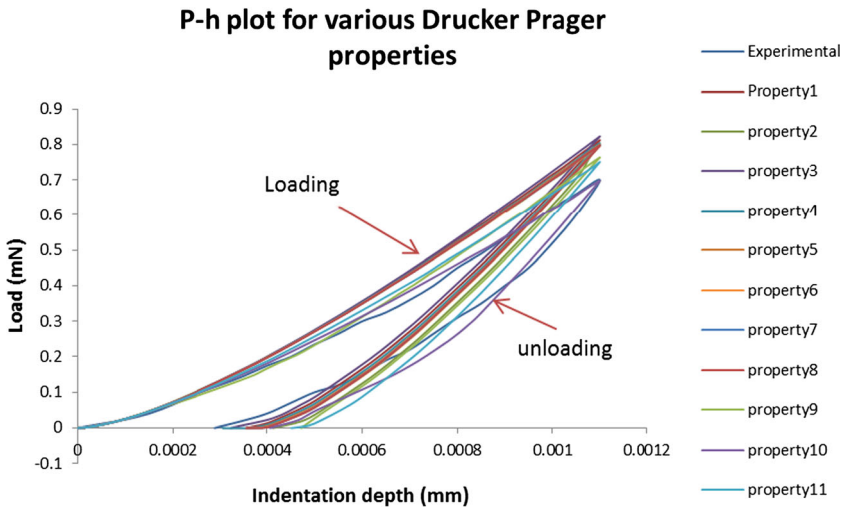

Fig. 6 Force displacement behaviour for different DP properties

friction formulation was adopted with a coefficient of friction of 0.2 for diamond-silicon contact, and hard contact was chosen to define contact pressure-overclosure relationship with constraint enforcement method as default.

2.2.3 Indentation test results and discussion

DP parametric evaluation was performed with more than 30 simulations by considering the effect of different values of friction angle, dilation angle and flow stress ratio. It has been observed that by increasing the friction angle β results in an increase in compressive strength of the material. Since the flow stress ratio range is limited by the $0.78 \leq K \leq 1$ condition and found to have very little effect on the load-displacement curve in this range, the most favourable K value of 0.82 was kept constant after verifying the effect.

Table 2 lists different selected properties with favourable results out of many other properties tested in this simulation study. The relevant parameters were selected which influence the model behaviour and offer a reasonable reduction in error difference between experimental and simulation results. In order to assess the dependency of the model on a certain parameter, other parameters were kept constant and the model was tested for varied parameter values.

The dilation angle Ψ relates to the volumetric strain during plastic deformation, and it remains constant during plastic yielding. The condition $\Psi = 0$ corresponds no volumetric strain, $\Psi > 0$ shows volume increase and $\Psi < 0$ signify a reduction in volume. Silicon exhibit volume reductions of 20–25 % [52] under loading when enduring pressure-induced phase transformation, corresponding to negative dilation angle. Stress, strain and other internal state variables are evaluated to characterise the material behaviour under loading and unloading conditions.

The hydrostatic pressure was measured for different DP parameters β and Ψ values in all the indentation tests, and the values of hydrostatic pressure were found to occur in the range of (8–19 GPa). Since this range lies in the structural transformation zone of silicon, plastic deformation would be the possible outcome leading to phase transformation in high-pressure range with little brittle fracture at low pressures. Indentation of silicon results in crack generation as well as

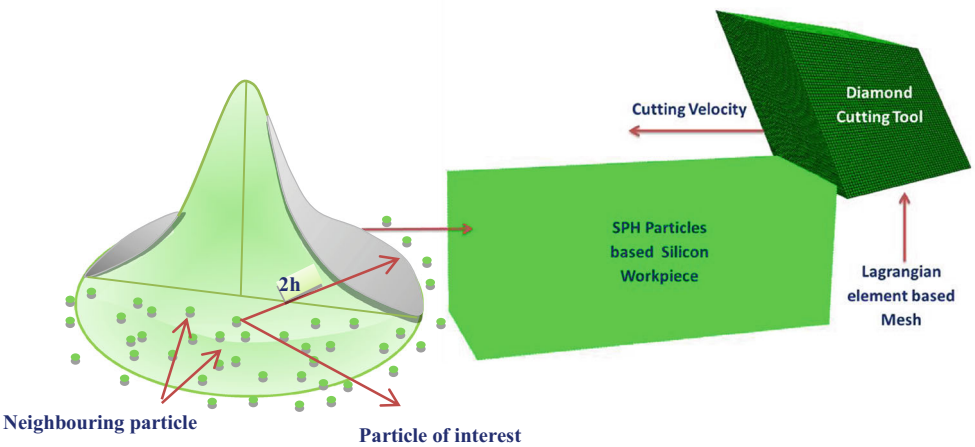

Fig. 7 SPH cutting model of single point diamond turning

Table 3 Material properties of silicon

Density (ρ)	2.3×10^{-9} tonne/mm^3
Elastic modulus (E)	155 GPa
Poison's ratio	0.2
Friction angle (β)	26
Dilation angle (Ψ)	−20
Flow stress ratio (k)	0.82

plastic deformation under pertained hydrostatic pressure. Crack generation in indentation test instigated at point where the fracture strength of the material dissolved by increased local maximum principal tensile stress.

Figure 5 shows the hydrostatic pressure for the DP parameters of property 10. Hydrostatic stress is the measure of average of three principal stress components and described as

$$\sigma = \frac{1}{3}(\sigma_1 + \sigma_2 + \sigma_3) \tag{8}$$

Where σ is the hydrostatic stress and σ_1, σ_2 and σ_3 are the stress components in three principal axes x, y and z, respectively. The hydrostatic stress gradient in the indentation zone was found to reach the highest under the indenter tip and reaches to 14 GPa for full indentation depth.

The variance effect in dilation angle Ψ and friction angle β on the hydrostatic pressure was also observed, and it was found that the hydrostatic pressure decreases with the increase in the negative dilation angle. Also with the increasing friction angle β, the hydrostatic pressure was found to increase.

Figure 6 presents load-displacement plot for different DP constitutive parameters. The values of each DP parameters were optimised periodically using trial and error method to remove the error difference between experimental and simulation results. The values of dilation angle changed between the two extremes to find the material load behaviour. Any increase in the negative dilation angle was found to decrease the reaction forces and any increase of friction angle was found to increase the reaction forces as well as the computational cost. In the simulation study, DP parameters of property 10 were found as unique parameters to achieve the required agreement (less than 4 % error) to the experimental curve.

2.3 SPH machining model of Silicon

SPH simulation model of conventional cutting was developed with negative rake angle tool. Figure 7 represents the SPH model of cutting process of diamond turning along with its kernel approximation. The cutting tool was modelled as a rigid tool using C3D8R elements. The silicon workpiece was modelled as a deformable part with dimensions of $360 \times 180 \times 100$ μm using PC3D elements to handle high deformation in cutting process. A convergence study was carried out based on von Mises stress to determine the optimal particles density for obtaining accurate simulation results with computational efficiency. The SPH particle density was kept homogeneous throughout the workpiece part in order to avoid any undesirable stress concentration. The bottom surface of the workpiece was kept fixed in all directions to achieve required stiffness. The depth of cut was 10 μm, and cutting velocity of 6.3 m/s was applied to the tool in the negative x-direction.

Table 3 lists the elastic and plastic properties of the material. Elastic-brittle/perfectly plastic response behaviour of silicon was investigated using pressure-dependent DP yield criterion.

The material model parameters obtained through inverse analysis were used to simulate the cutting process. SPH can simulate the chip separation naturally and therefore chip separation was achieved without introducing any physical, geometrical separation criteria or damage model. The simulation model analyses the mechanical interaction between silicon workpiece and diamond tool. In cutting operation, the slip between different layers of atom results in chip formation and cutting is mainly subsidised due to the shearing action.

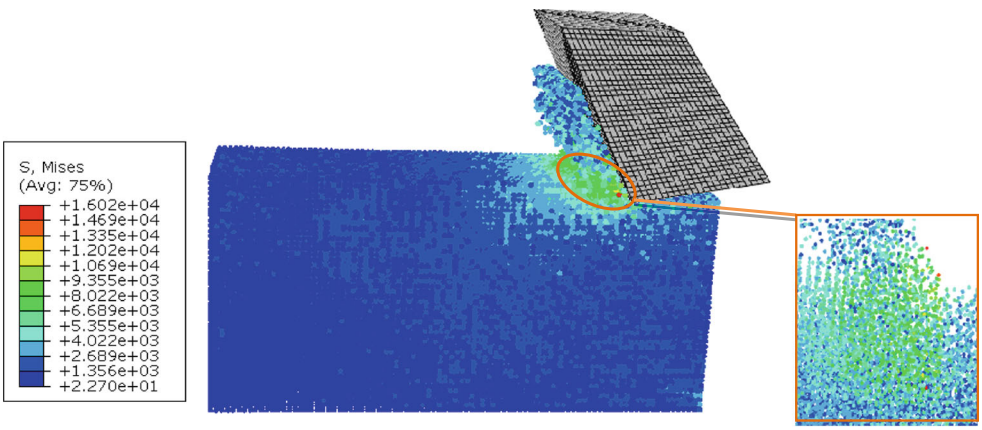

Fig. 8 SPH cutting simulation of silicon with von Mises stresses (MPa)

Table 4 Experimental data: material specification and cutting parameters

Silicon	Crystal orientation	<111>
	Wafer size	Dia = 100 mm, thickness = 5 mm
Diamond	Crystal orientation	Dodecahedral
	Rake angle	−25°
	Clearance angle	10
	Nose radius	5 mm
Cutting parameters	Speed	1200 rpm
	Feed	1 μm/rev
	Depth of cut	10 μm
	Coolant	Water mist

Figure 8 illustrates chip formation of silicon at the steady-state condition. The chip formation was observed with the combination of plastic deformation in the chip formation zone with minor brittle fracture on the free chip surface. The von Mises stresses reached beyond yield strength of silicon showing machining through plastic deformation.

2.4 Experimental validation of SPH model

In order to assess the validity of the developed SPH simulation model, diamond turning of single crystal silicon was performed and cutting forces results were compared with the simulation results. Silicon with crystal orientation (111) was machined using Precitech Nanoform 250 ultra-precision diamond turning machine.

Single crystal diamond tool with round edge was used to machine silicon. Silicon is known to expedite high tool wear during machining ensuing shorter tool life and degradation of surface quality. Since the surface depreciation also attributed to pre-machining cracks and crack initiation in the primary shear zone and their propagation into the machined surface, the silicon wafer was carefully observed for any pre-machining defects and surface cracks.

Table 4 lists the specification of the silicon wafer and diamond tool along with cutting parameters used in the machining experiments. Diamond tool was examined under SEM for any prior damage before diamond turning. Cutting forces developed during machining were monitored and recorded using three-component Kistler dynamometer 9256, charge amplifier and an advanced data acquisition system with Dynoware. Figure 9 shows the machining setup of diamond turning of silicon.

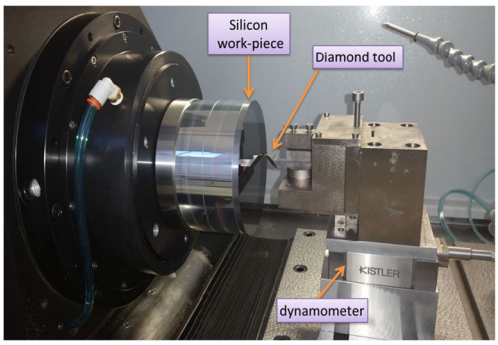

Fig. 9 Machining setup for diamond turning silicon

2.5 Cutting forces result comparison

In order to avoid any inconsistency in machining and simulation model, the cutting velocity, depth of cut and rake and clearance angle are kept in the same values in both studies. In machining, cutting forces significantly influence by tool-chip interface friction parameters, material properties as well as tool geometry [53]. Classical Coulomb's friction model has been widely used in machining due to its simplicity and has a significant effect on the magnitude of cutting forces. The friction coefficient between diamond and silicon in machining is always approximated and has not yet been identified with certainty [54]. In SPH, a tool-chip interface friction criterion is governed by the interaction of stressed particle and its effective neighbouring particles. SPH, therefore, offers internal friction criteria of the particles between the tools and the workpiece when both are modelled with SPH particles, and therefore, no Coulomb's friction coefficient is required. However, Abaqus does not allow the interaction of two different SPH particles parts; the tool was modelled with Lagrangian mesh-based approach. Penalty friction formulation with a friction

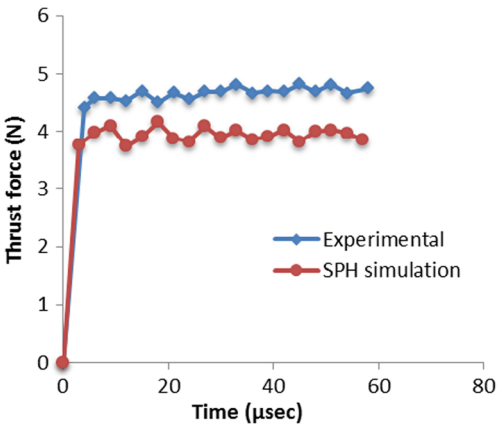

Fig. 10 Thrust forces comparison of experimental and simulation model

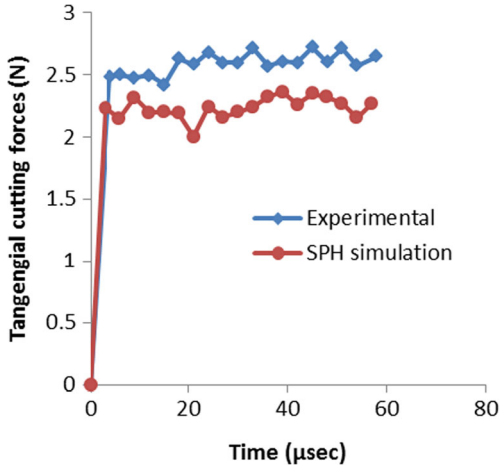

Fig. 11 Tangential force comparison of experimental and simulation model

coefficient of 0.2 was used in SPH machining model. Cutting forces were recorded for both experimental work and simulation model.

Figures 10 and 11 show the comparison of thrust forces and tangential cutting forces, respectively, obtained through experimental and simulation studies. In both the experimental and simulation model, cutting forces increase sharply as the tool makes contact with the workpiece. After the initial chip formation stage, the forces remain stable with slight variation indicating steady-state cutting. It can be seen that in the experimental study, both tangential and thrust forces are slightly higher than the simulation model. The percentage difference in the average tangential and thrust forces obtained from experimental and SPH results was measured in the equitable range of 12.8 and 13.2 %, respectively. The differences between the simulated cutting forces with those obtained through cutting trials are due to ideal (no internal defects) diamond tool and silicon workpiece are assumed and machine stiffness effects were not considered in order to reduce the complexity of simulation model.

3 Surface defect machining simulation

Results from SPH simulations of conventional and SDM machining of silicon were compared and any transition in the cutting forces, material removal behaviour and stress distribution were investigated to evaluate the SDM approach. Surface defects of different types were introduced onto the workpiece top surface of validated SPH model. Both conventional and SDM machining simulations were carried out with similar cutting parameters and tool geometry. The particle density was maintained virtually homogeneous around the defects in order to avoid any artificial stress concentration as well as to maintain sufficient particle resolution around the defects.

Figure 12 presents the different type of surface defects used to evaluate the surface defect machining of silicon. Surface defects were equally distributed on the top surface of the workpiece with an internal distance of 10 µm. Table 5 list the dimensions of defects exploited in SDM study along with model details.

4 Results and discussion

4.1 Chip formation

In the conventional metal cutting process, chip formation is due to the shearing action in which layer of front atoms slip over the subsequent layer of atoms [55]. In machining silicon, the chip formation is usually through a combination of plastic deformation and brittle fracture resulting in a mixture of continuous and discontinuous chips (dependent upon hydrostatic pressure). In diamond turning trial in this study, the depth of cut is controlled below brittle to ductile transition point. Silicon chips were therefore removed in ductile mode and good surface finish of 5 nm was achieved. Figure 13 shows continuous chips obtained during machining trials.

Figure 14 shows the chip formation as well as the distribution of von Mises stress in conventional and SDM machining with different type of pre-formed defects.

The maximum value of von Mises stress reached ~16 GPa in conventional machining whereas the stresses in SDM machining reduced for all the defects. The maximum reduction in von Mises stress was observed in vertical defects for which the highest value reached 14.6 Gpa.

In conventional machining, when no defects are present, the atoms on the uncut chip layer intact with each other provide strength to the material. Due to this bonding strength, reaction to any induced stresses results in the resistance to deformation by the layer of atoms present in front of the tool cutting edge. The front atomic layer transfers the stress energy to the following unstressed layer of atoms and causes stresses

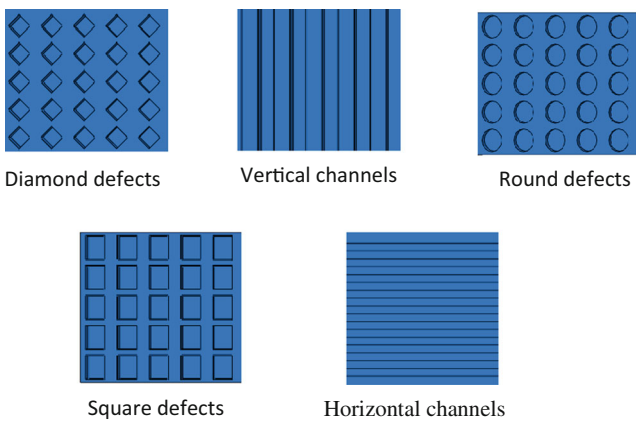

Fig. 12 Surface defect patterns in SDM simulations

Table 5 Specification of SPH conventional and SDM simulation models

Machining	Model dimensions (μm)	Width/diameter (μm)	Defect depth (μm)	Depth of cut (μm)	SPH particles
Conventional	360 × 180 × 100	N/A			134,877
Horizontal	360 × 180 × 100	15 × 360	8	10	134,695
Vertical	360 × 180 × 100	15 × 100	8	10	136,991
Diamond	360 × 180 × 100	15 × 15	8	10	140,531
Square	360 × 180 × 100	15 × 15	8	10	147,181
round	360 × 180 × 100	15	8	10	165,123

to develop in the larger area in front of the tool as well as an increase in shear strength of material. This, therefore, results in brittle fracture in the weak zone due to anisotropic strength property of the material. Depending on the rake angle of the tool, this phenomenon transpires in the surface layer in front of the positive rake tool as well as front and under the surface in the negative rake angle tool.

In SDM machining, this front atomic surface layer can only pass partial strain energy to the unstressed atoms due to the defects present between the layers results in chip formation with less cutting force and less influenced area. Depending on the defects type, stress distribution localises within chip formation zone which also facilitates chip reduction in the secondary deformation zone. In SDM machining, the material removal in front of the cutting edge remains continuous, whereas, on the free surface of the chip, it removes through brittle fracture. The disintegration of particles in SDM machining on the free surface side of the chip can be observed in Fig. 14 compared with conventional machining in which the particles of the chip are more compact and connected. This brittle failure on the free surface of the chip offers a reduction in cutting resistance. In conventional machining, where plastic deformation is dominant on both sides of the chip, silicon offers high resistance to plastic deformation and therefore requires high energy and result in higher cutting forces in plastic deformation than brittle fracture.

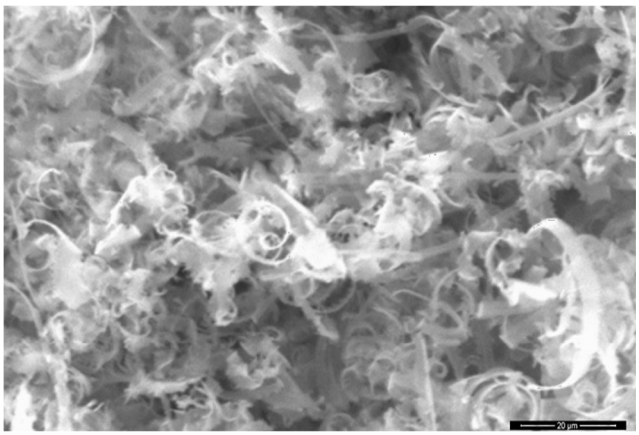

Fig. 13 Continuous chips obtained in machining silicon

4.2 Primary shear zone

The schematic of conventional cutting with chip formation and illustration of primary and secondary shear zone is presented in Fig. 15. Shear stresses, strain rate and temperature are significantly influenced by the change in geometry of primary shear zone [56]. The geometry of the primary shear zone is governed by the shear plane angle ($\varnothing_s$) and the ratio of the length of the primary shear zone (l_{AB}) to its thickness (t_p).

The shear strain prevails in primary shear zone area with maximum strain at plane AB. The strain AB is described in Eq. 9.

$$\varepsilon_{AB} = \frac{\cos\alpha}{2\mathrm{Sin}\varnothing_s \cos(\varnothing_s - \alpha)} \tag{9}$$

In Eq. 9, ε_{AB} is shear strain in the primary shear plane AB. The angle α is the rake angle of the tool and φ_s is the shear plane angle.

Figure 16 shows the comparison of shear plane length for the conventional and SDM machining with vertical and square defects. A significant reduction in shear plane length can be observed from 14 μm in conventional to a maximum of 8 and 11 μm when machining with vertical and square defects, respectively. The shear plane length varies with reference to defect position and reduces to 4 μm near the defect area. Chip length in the secondary deformation zone was also found to reduce in SDM machining compared with conventional machining.

The variation in primary shear zone geometry in three different types of defects (including analogous V-type defect for illustration purpose) is explained in Fig. 17. It can be seen that in all three types of surface defects, the length of the shear plane (l_{AB}) reduced in slight disparity as well as reduction in shear plane area. The shear plane length varies sequentially throughout the cutting distance travelling through continuous-defect-continuous areas, whereas in conventional machining, this length remains constant throughout the cutting distance. Shear plane area and shear strain magnitude increase when using negative rake angle tool [57] result in higher cutting forces.

In SDM, the depreciation in the shear plane area contributes to the reduction of shear strength of the material in the

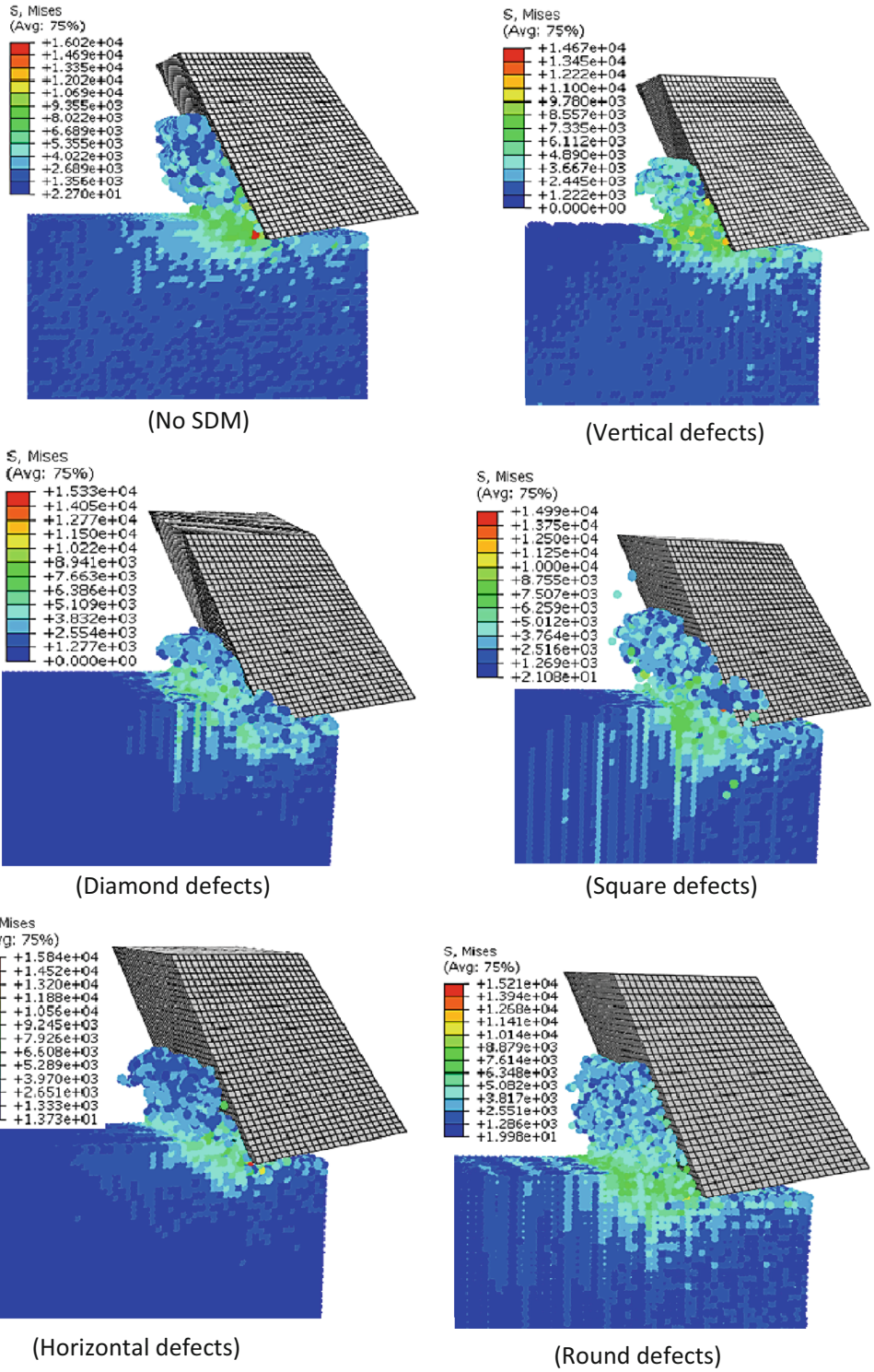

Fig. 14 Chip formation and von Mises stress (MPa) in conventional and SDM machining

primary shear zone. The shortening of shear plane length in the primary shear zone also reduces the secondary shear zone eventually reducing cutting resistance. In the primary shear area a–b–c in all three defects, the length of the upper region (l_{ab}) is shorter than the length of the lower region ((l_{ac}) and therefore endure high strain rate in upper regions than the lower region. Chip separation starts from smaller high-stress state region (zone I) towards larger region (zone II) with maximum stress concentration in both zones. The shape of the region II governs the chip thickness and length. The variation

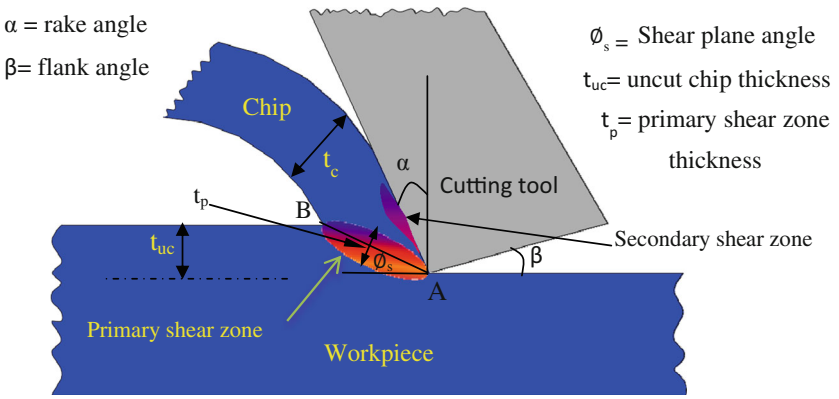

Fig. 15 Schematic of chip formation conventional cutting

of zone II in square, round and v-type defects offers varied cutting resistance and therefore the difference in chip morphology.

4.3 Cutting forces

Figure 18 encompasses the comparison of normal force for multiple surface defects recorded against regular time steps during cutting simulations. The variation in cutting forces trend for multiple surface defects ascertains varied cutting resistance offered by different defects type. The cutting resistance of the material is overwhelmed by the cutting force component (F_c) whereas the negative rake angle of the tool compresses the material layer and causes increase in normal force component (F_n) on the tool [58]. In conventional machining, the cutting force originates with a sharp increase at initial tool contact with the workpiece. The magnitude of cutting force increases during material separation and results in

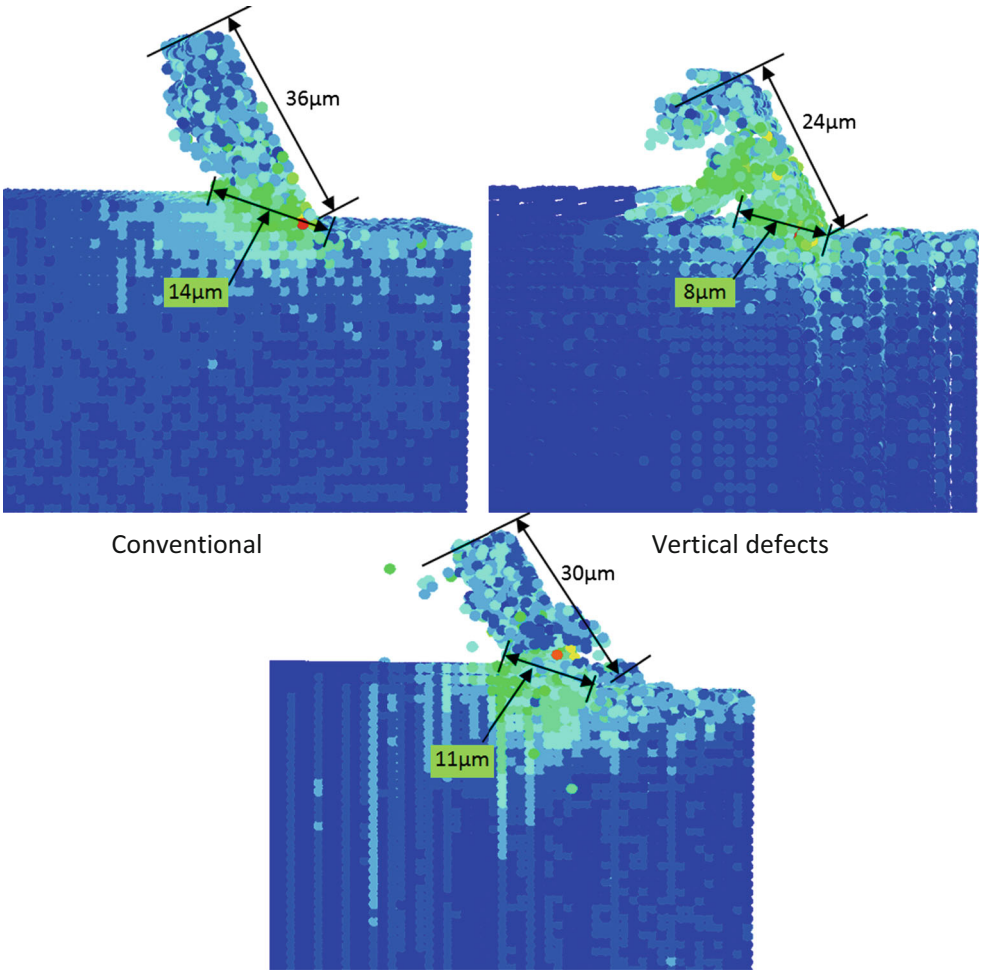

Fig. 16 Comparison of shear plane length in conventional machining and in SDM with vertical defects

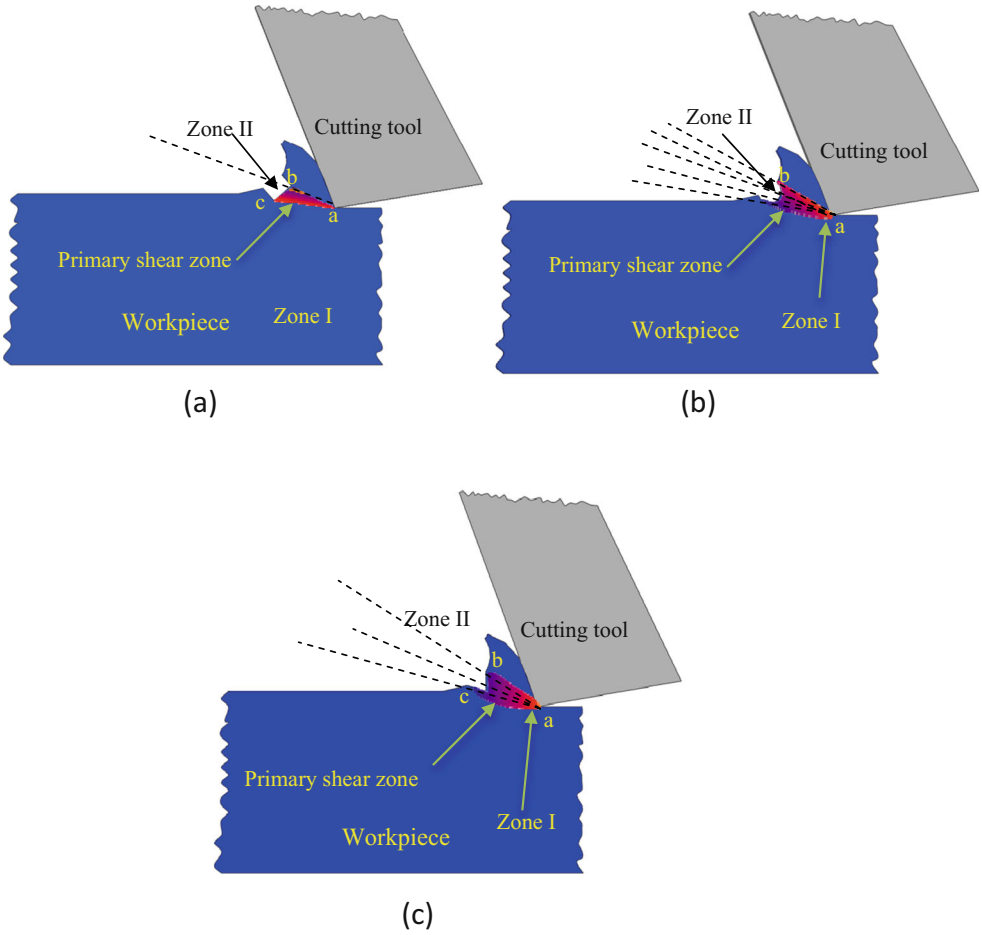

Fig. 17 Primary shear zone geometry in SDM machining **a** square, **b** round and **c** V-type defects

preliminary chip separation from the workpiece and reaching a maximum value. The cutting force stabilises with little disparity due to continuous machined surface in the succeeding cutting.

The SDM process characterised by unique defects forming variable contact pressure and cutting resistance and therefore undergo different cutting force trend. With the initial tool contact with the workpiece surface, the cutting force increases until tool reaches the defect area where the tool faces less resistance due to sporadic contact with the workpiece surface. The cutting force magnitude in all SDM simulations was established lower in comparison with conventional machining. In conventional diamond turning silicon, although the chip morphology is hydrostatic pressure dependent and obtains in the combination of ductile and brittle fracture, in SDM machining, brittle fracture is dominant on the free surface of

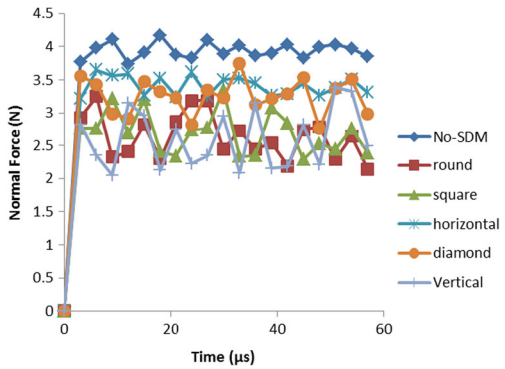

Fig. 18 Normal force trend of conventional and SDM machining simulation

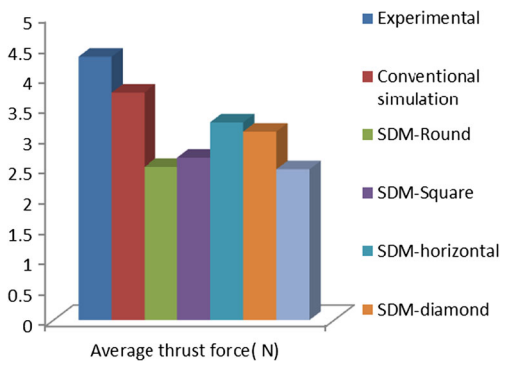

Fig. 19 Average thrust force comparison of conventional experimental, simulation and SDM methods

the chip. This also reduces the secondary shear zone length which consequently reduces the cutting forces [59]. In the horizontal SDM simulation, the highest cutting forces were obtained from other defect type simulations. This is due to the defects existing parallel to the cutting direction which does not considerably affect primary and secondary shear zone area. It can also be observed from Fig. 18 that each defect offers a different force magnitude with square and round defects offering the lower cutting forces.

A comparison of average thrust force magnitudes in all simulations and experiments was presented in Fig. 19, substantiating the effectiveness of SDM method.

5 Conclusions

SPH simulations of orthogonal cutting of conventional and SDM method have been carried out to establish the effectiveness of recently developed SDM method in diamond turning silicon. The efficacy of SDM method was demonstrated by evaluating the material response behaviour under conventional and SDM machining approaches. Cutting forces and steady-state chip formation in different defect type simulations were studied. The study reveals that SDM can be effectively exploited to attain better surface finish and reduced tool wear in single point diamond turning process. The results from the experimental and simulation study can be concluded as follows:

1. Surface defects on the workpiece surface reduce the shear plane area and shear plane length of the primary deformation zone. This phenomenon contributes to lowering the shear strength of the material in the chip formation zone which helps in relaxed chip formation and lower cutting temperature.
2. SDM approach offers reduction in the cutting resistance of the material and therefore a decrease in the cutting energy. Consequently, it reduces diamond tool wear and improves surface finish.
3. The decrease in chip length during SDM machining contributes in reducing the secondary deformation zone length and hence reduced tool wear.

Acknowledgments The authors would like to thank EPSRC (EP/K018345/1) and Royal Society-NSFC International Exchange Scheme for providing financial support to this research.

References

1. King RF, Tabor D (1954) The strength properties and frictional behaviour of brittle solids. Proc Roy Soc Lond Ser Math Phys Sci 223(1153):225
2. Morris JC et al (1995) Origins of the ductile regime in single-point diamond turning of semiconductors. J Am Ceram Soc 78(8):2015–2020
3. Zarudi I et al (2004) The R8-BC8 phases and crystal growth in monocrystalline silicon under microindentation with a spherical indenter. J Mater Res 19(1):332–337
4. Patten J, Gao W, Yasuto K (2005) Ductile regime nanomachining of single-crystal silicon carbide. J Manuf Sci Eng 127(3):522
5. Blackley WS, Scattergood RO (1991) Ductile-regime machining model for diamond turning of brittle materials. Precis Eng-J Am Soc Precis Eng 13(2):95–103
6. Durazo-Cardenas I et al (2007) 3D characterisation of tool wear whilst diamond turning silicon. Wear 262(3-4):340–349
7. Rusnaldy, Ko TJ, Kim HS (2007) An experimental study on microcutting of silicon using a micromilling machine. Int J Adv Manuf Technol 39(1-2):85–91
8. Tang X et al (2013) Ultraprecision micromachining of hard material with tool wear suppression by using diamond tool with special chamfer. CIRP Ann Manuf Technol 62(1):51–54
9. Tanaka H, Shimada S (2013) Damage-free machining of monocrystalline silicon carbide. CIRP Ann Manuf Technol 62(1):55–58
10. Suzuki H et al (2013) Development of micro milling tool made of single crystalline diamond for ceramic cutting. CIRP Ann Manuf Technol 62(1):59–62
11. Wang ZY, Rajurkar KP (2000) Cryogenic machining of hard-to-cut materials. Wear 239(2):168–175
12. Ghosh R (2006) Technology assessment on current advanced research projects in cryogenic machining. 1–87
13. Umbrello D, Micari F, Jawahir IS (2012) The effects of cryogenic cooling on surface integrity in hard machining: a comparison with dry machining. CIRP Ann Manuf Technol 61(1):103–106
14. Kumar MN et al (2014) Vibration assisted conventional and advanced machining: a review. Procedia Eng 97:1577–1586
15. Skelton RC (1967) Turning with an oscillating tool. Int J Mach Tool Des Res 8:239–259
16. Brehl DE, Dow TA (2008) Review of vibration-assisted machining. Precis Eng 32(3):153–172
17. Venkatesan K, Ramanujam R, Kuppan P (2014) Laser assisted machining of difficult to cut materials: research opportunities and future directions—a comprehensive review. Procedia Eng 97:1626–1636
18. Xavierarockiaraj S, Kuppan P (2014) Investigation of cutting forces, surface roughness and tool wear during laser assisted machining of SKD11Tool steel. Procedia Eng 97:1657–1666
19. Rahman Rashid RA et al (2012) An investigation of cutting forces and cutting temperatures during laser-assisted machining of the Ti–6Cr–5Mo–5V–4Al beta titanium alloy. Int J Mach Tool Manuf 63:58–69
20. Mohammadi H et al (2015) Experimental work on micro laser-assisted diamond turning of silicon (111). J Manuf Process 19:125–128
21. Rashid WB et al (2013) The development of a surface defect machining method for hard turning processes. Wear 302(1-2):1124–1135
22. Rashid WB et al (2013) An experimental investigation for the improvement of attainable surface roughness during hard turning process. Proc Inst Mech Eng, Part B: J Eng Manuf 227(2):338–342
23. Jackson MJ, Robinson GM (2005) High strain rate induced initial chip formation of certain metals during micromachining processes. Mater Sci Technol 21(3):281–288
24. Priyadarshinin A, Samantaray AK (2012) Finite element modeling of chip formation in orthogonal machining. In: Davim JP (ed) Statistical and computational techniques in manufacturing. London.

25. Carroll JT, Strenkowski JS (1988) Finite-element models of orthogonal cutting with application to single point diamond turning. Int J Mech Sci 30(12):899–920
26. Movahhedy M, Gadala MS, Altintas Y (2000) Simulation of the orthogonal metal cutting process using an arbitrary Lagrangian-Eulerian finite-element method. J Mater Process Technol 103(2): 267–275
27. Gong Y (2010) Meshless methods in LS DYNA: an overview of EFG and SPH. in LS DYNA seminar. Livermore Software Technology Corporation, Stuttgart
28. Uhlmann E, Gerstenberger R, Kuhnert J (2013) Cutting simulation with the meshfree finite pointset method. Procedia CIRP 8:391–396
29. Gingold RA, Monaghan JJ (1977) Smoothed particle hydrodynamics: theory and application to non shperical stars. Mon Not R Astron Soc: 375–389
30. Cleary PW, Prakash M, Ha J (2006) Novel applications of smoothed particle hydrodynamics (SPH) in metal forming. J Mater Process Technol 177(1–3):41–48
31. Rüttimann N et al (2013) Simulation of hexa-octahedral diamond grain cutting tests using the SPH method. Procedia CIRP 8:322–327
32. Das R, Cleary PW (2010) Effect of rock shapes on brittle fracture using smoothed particle hydrodynamics. Theor Appl Fract Mech 53(1):47–60
33. Bui HH et al (2008) Lagrangian meshfree particles method (SPH) for large deformation and failure flows of geomaterial using elastic-plastic soil constitutive model. Int J Numer Anal Methods Geomech 32(12):1537–1570
34. Lin J et al (2014) Efficient meshless SPH method for the numerical modeling of thick shell structures undergoing large deformations. Int J Non Linear Mech 65:1–13
35. Nordendale NA, PK Basu, Heard WF (2013) Modeling of high rate ballistic impact of brittle armors with abaqus explicit. In: Simulia Community Conference, Vienna, Austria
36. Villumsen MF, Fauerholdt TG (2008) Simulation of metal cutting using smooth particle hydrodynamics. in LS-DYNA: metallumformung III. Anwenderforum, Bamberg
37. Zhao H et al (2013) Influences of sequential cuts on micro-cutting process studied by smooth particle hydrodynamic (SPH). Appl Surf Sci 284:366–371
38. Gasiorek D (2013) The application of the smoothed particle hydrodynamics (SPH) method and the experimental verification of cutting of sheet metal bundles using a guillotine. J Theor Appl Mech 51(4):1053–1065
39. Xi Y et al (2014) SPH/FE modeling of cutting force and chip formation during thermally assisted machining of Ti6Al4V alloy. Comput Mater Sci 84:188–197
40. Limido J et al (2007) SPH method applied to high speed cutting modelling. Int J Mech Sci 49(7):898–908
41. Calamaz M et al (2009) Toward a better understanding of tool wear effect through a comparison between experiments and SPH numerical modelling of machining hard materials. Int J Refract Met Hard Mater 27(3):595–604
42. Okhrimenko GM (1989) Single crystal silicon piezoelectric ceramics and ferrite under uniaxial compression. Problemy Prochnosti 9:45–80
43. Wan H et al (2011) A plastic damage model for finite element analysis of cracking of silicon under indentation. J Mater Res 25(11):2224–2237
44. Drucker DC, Prager WJ (1952) Soil mechanics and plastic analysis or limit design. Brown University, Division of Applied Mathematics
45. Simulia (2014) User documentation, Abaqus 6.14 Software manual
46. Seltzer R et al (2011) Determination of the Drucker–Prager parameters of polymers exhibiting pressure-sensitive plastic behaviour by depth-sensing indentation. Int J Mech Sci 53(6):471–478
47. Yoshino M et al (2001) Some experiments on the scratching of silicon: in situ scratching inside an SEM and scratching under high external hydrostatic pressures. Int J Mech Sci 43(2):335–347
48. Jang J-I et al (2005) Indentation-induced phase transformations in silicon: influences of load, rate and indenter angle on the transformation behavior. Acta Mater 53(6):1759–1770
49. Zarudi I, Zhang LC (1999) Structure changes in mono-crystalline silicon subjected to indentation experimental finding. Tribol Int 32: 701–712
50. Juliano T, Domnich V, Gogotsi Y (2011) Examining pressure-induced phase transformations in silicon by spherical indentation and Raman spectroscopy: a statistical study. J Mater Res 19(10): 3099–3108
51. Cao YP, Dao M, Lu J (2011) A precise correcting method for the study of the superhard material using nanoindentation tests. J Mater Res 22(05):1255–1264
52. Kailer A, Gogotsi YG, Nickel KG (1997) Phase transformations of silicon caused by contact loading. J Appl Phys 81(7):3057
53. Özel T (2006) The influence of friction models on finite element simulations of machining. Int J Mach Tool Manuf 46(5):518–530
54. Yan J, Zhao H, Kuriyagawa T (2009) Effects of tool edge radius on ductile machining of silicon: an investigation by FEM. Semicond Sci Technol 24(7):075018
55. Fang N, Jawahir IS (2002) Analytical predictions and experimental validation of cutting force ratio, chip thickness, and chip back-flow angle in restricted contact machining using the universal slip-line model. Int J Mach Tools Manuf 42(6):681–694
56. Pang L, Kishawy HA (2012) Modified primary shear zone analysis for identification of material mechanical behavior during machining process using genetic algorithm. J Manuf Sci Eng 134(4):041003
57. Lee S et al (2005) Large strain deformation field in machining. Metall Mater Trans 37(A):1633–1643
58. Fang N (2005) Tool-chip friction in machining with a large negative rake angle tool. Wear 258(5-6):890–897
59. Cubberley WH, Bakerjian R (1989) Tool and manufacturing engineers handbook, ed. S.o.M.E. (SME). USA